

Study on Laser Cleaving Mechanism of Brittle Materials

メタデータ	言語: English 出版者: 公開日: 2017-10-05 キーワード (Ja): キーワード (En): 作成者: アリヤス, ビン モハマド サマン, Alias, Bin, Mohd, Saman メールアドレス: 所属:
URL	http://hdl.handle.net/2297/42265

This work is licensed under a Creative Commons Attribution-NonCommercial-ShareAlike 3.0 International License.



学位論文要旨

**Study on the Laser Cleaving Mechanism
of Brittle Materials**

レーザーによる硬脆材料の切断メカニズムに関する研究

Graduate School of Natural Science & Technology, Kanazawa University

Division of Innovative Technology and Science

System Design and Planning

Alias bin Mohd Saman

Study on the Laser Cleaving Mechanism of Brittle Materials

Abstract

This paper describes the investigation of the laser cleaving mechanism of brittle materials such as silicon wafer using experimental and computational methods. The applied laser energy produces a thermal stress that causes the wafer to split along the irradiation path. The wafer separation is similar to crack extension. In this study, the use of micro-groove was introduced, and the influences of groove length and depth were also examined. The temperature of the laser spot was measured using a two-colour pyrometer, while the fracture occurrences were observed by monitoring the acoustic emission signal. The relationships amongst laser power, temperature, fracture initiation, crack propagation, cleaved surface features and groove parameters are obtained from the experimental analysis. In order to understand the stress condition during laser irradiation, thermal stress distribution was analysed using the computational finite element method (FEM). The results indicate that the wafer separation occurred in two stages, fracture initiation and intermittent crack propagation. A higher temperature resulted in faster fracture initiation and higher repetition of the crack propagation signal. The wave mark on the cleaved surface was consistent with the AE signal. By using FEM, stress condition has been quantitatively determined by identifying the stress intensity factor K_I . Fracture toughness K_{IC} of the material has been determined experimentally using the Vickers indentation technique.

1. Introduction

Laser cleaving is a process used for separating a brittle material by irradiating a laser beam on a small area of the substrate. In this technique, the applied laser energy produces a thermal stress that causes the material to separate along the moving path of the laser beam. The material separation is similar to a crack extension, and the fracture growth is controllable. The material separation process is similar to crack extension. This process is preferred over the conventional mechanical dicing process due to its non-contact cutting process. The process does not need a coolant and the production of chips is eliminated. Furthermore, this method is capable of producing an excellent surface finish.

The first application of the laser in separating brittle materials such as alumina ceramic and glass was proposed by Lumley using a controlled fracture technique [1]. This procedure uses less laser power and enables high cutting speeds compared to conventional laser cutting methods. Later, the use of two lasers was developed to separate the glass [2]. The first laser beam was used to create a shallow groove via heating and vaporizing procedures. The second laser beam generated thermal stress at the groove tip to separate the material. The fracture mechanism of alumina material by laser cleaving was investigated using a single laser [3]. A shallow groove was created by using an evaporative procedure, and heat produced by the laser beam generated a time-dependent thermal stress along the moving path.

Several studies have been performed on the thermal cleaving process of a silicon wafer. It was found that the temperature of the area irradiated

with a pulsed laser is an important factor in controlling the propagation of the crack and in achieving high cleaving accuracy with little thermal damage [4]. Therefore, a cleaving process with a pulsed laser and the use of refrigerating chuck for cleaving with a continuous wave (CW) laser are recommended to reduce thermal damage during the cleaving processes [5]. Additionally, separation of silicon wafer material in the same direction as the wafer cleavage plane can be achieved by lower laser energy, further improving the cleaving surface [6].

The investigations on the laser cleaving of a silicon wafer were previously performed with the used of the initial crack that was prepared using Vickers indenter impressions. However, the impression creates damage in the indentation area and a lateral crack in the direction perpendicular to the cleaving path. Therefore, in this study, the use of a micro-groove to facilitate the fracture initiation during laser cleaving process is introduced. The unnecessary crack and damage were eliminated during the initial crack preparation, subsequently improving the quality of the material specimen. In previous research, the studies were concentrated on the laser cleaving performances, the thermal damages and the influences of crystal orientation of the material. However, a limited study on the processing mechanism in laser cleaving of brittle materials such as silicon has also been reported.

In this paper, the laser cleaving mechanism of a silicon wafer using a moving laser beam is investigated experimentally and computationally. The micro-groove was prepared at the leading edge of the silicon wafer to facilitate the fracture. The influence of the groove parameters, such as groove length and depth, is also studied. The temperature

of the laser spot was measured using a two-color pyrometer, while the fracture occurrences were observed by monitoring the acoustic emission signal. The cleaved surface was observed using scanning electron microscope (SEM). Therefore, the relationships between laser power, temperature, fracture initiation, crack propagation, cleaved surface features and groove parameters are described. In order to explain the thermal stress distribution during laser irradiation, the finite-element method (FEM) software, ANSYS, is applied.

2. Experimental Methodology

2.1 Silicon wafer specimen

The specimen used in the experiments was a silicon wafer of <100> crystal orientation and a thickness of 0.5 mm. The schematic illustration of the silicon wafer specimen with a size of 20 mm x 10 mm x 0.5 mm is shown in Fig. 1. The micro-groove was created at the edge of the silicon wafer by focusing the pulsed laser beam through the micro-lens. A second harmonic generation (SHG) Nd:YAG laser with a wavelength of 532 nm, frequency of 10 Hz and pulse width of 5 nsec was used in the specimen preparation. The laser energy was focused into the specimen resulting in material heating and evaporating, thus forming the groove. By using this technique, the groove size can be controlled, and the area of damage was very small.

The depth of the groove was adjusted by varying the laser pulse number while the groove length was controlled by focusing the laser beam only on the required exposed area. Fig. 2 shows the relationship between the groove depth and laser pulse number. The images of the pre-prepared micro-groove are shown in Fig. 3.

2.2 Experimental procedure

In this experiment, the temperature of the laser spot was measured using a two-color pyrometer with optical fiber that was developed by Ueda et al. [7], while the AE signals were measured using the AE sensor to observe the crack propagation during the laser irradiation process. The experimental arrangement is illustrated in Fig. 4.

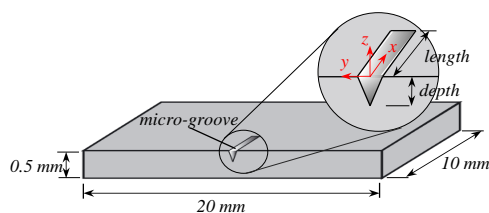


Fig. 1 Schematic illustration of the specimen with micro-groove

The continuous wave Nd:YAG laser with the wavelength of 1.06 μm was used as a heat source. The laser beam spot of 0.25 mm x 0.19 mm (oval shape) was defocused on the wafer's surface.

A chalcogenide optical fiber was set at a distance of 3 mm from the laser spot and an angle of 45° from the optical axis. The infrared energy radiated from the object was captured by a chalcogenide optical fiber and transmitted to a two-color pyrometer consisting of InSb and MCT detectors. The infrared energy was converted to an amplified electric signal. By calculating the ratio of output voltages from these two detectors, the temperature of an object was obtained using the calibration curve as shown in Fig. 5. An AE sensor was fixed on the wafer's surface at a distance of 5 mm from the micro-groove.

The output voltages from the pyrometer detectors and AE sensor were recorded in a digital oscilloscope. The laser power used for this experiment varied between 50 W and 70 W while the groove length and the depth were maintained at 500 μm and 80 μm accordingly. The scan speed was set at 2 mm/s. The separating surface was analysed using a scanning electron microscope (SEM). A summary of the experimental conditions is shown in Table 1.

3. Experimental Result and Discussion

3.1 Temperature measurement

Typical temperature profiles of the laser irradiation and AE signal are shown in Fig. 6. The temperature history of the laser spot along the irradiation path is shown in Fig. 6(a). It was found that higher temperature of the laser spot resulted in a position near to the edge of the silicon wafer.

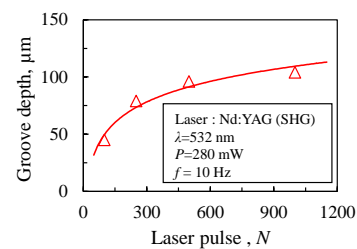


Fig. 2 Relation between laser pulse number and groove depth

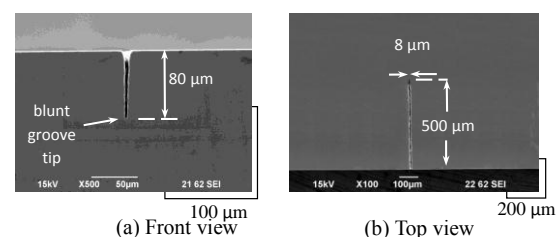


Fig. 3 Images of micro-groove with dimensions

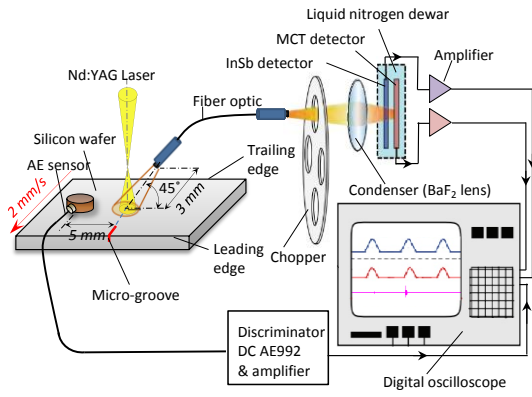


Fig. 4 Schematic illustration of experimental arrangement

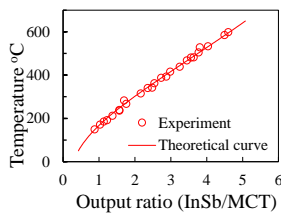


Fig. 5 Calibration curve

Table 1 Experimental condition

Laser	Nd :YAG laser	
Laser mode	Continuous wave	
Wavelength, λ	1.064	[μm]
Laser power, P	50 ~70	[W]
Beam size, $D1 \times D2$	0.25 x 0.19	[mm]
Moving speed, v	2	[mm/s]
Specimen	Silicon wafer	
Crystal orientation	<100>	
Size	10 x20 x0.5	[mm]
Pyrometer	Two-color pyrometer	
Detectors	InSb, MCT	
Optical fiber	NSEG	
Fiber core diameter, ϕ	380	[μm]

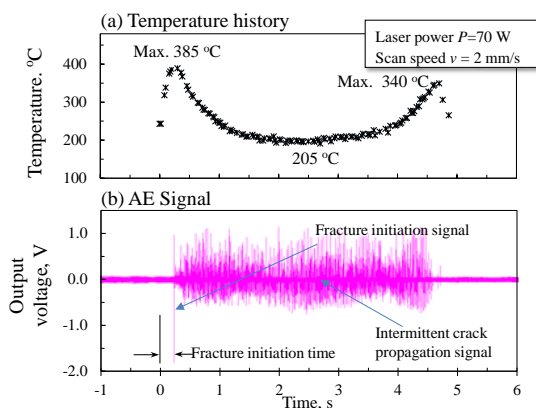


Fig. 6 Temperature history and AE signals

The maximum temperature of 385°C was recorded at approximately $t=0.27$ s. The temperature at the middle of the specimen was approximately 205°C, while the temperature of the laser spot rose to 340°C at approximately $t=4.73$ s. The results indicated that the laser spot was maintained at a constant lower temperature at the centre of the laser path. Silicon wafer has a high thermal conductivity of 156 W/m.K [5,8]. Hence, the energy produced by laser irradiation was circumferentially diffused efficiently when the laser beam was at the central area of the wafer.

The variation of maximum temperatures at the leading edge and the trailing edge, and the average temperature at the center of the specimen with the laser power are shown in Fig. 7. The temperature at all three positions increased with the increase of laser power. From the results, it is clear that the temperature of the moving laser spot was dependent on the energy supplied by the laser beam. High laser power resulted in an increase of temperature.

3.2 Acoustic emission (AE) signal

The signal from the AE sensor during laser beam irradiation is displayed in Fig. 6(b). Signals from the AE sensor demonstrated that the crack occurrences appeared in two stages, namely fracture initiation and intermittent crack propagation. AE signals were produced when a rapid release of energy from localized sources within the material occurred. Energy release occurred as a result of crack extension due to the thermal stress generated by the laser beam. The first signal of the AE wave showed that the fracture initiation occurred with larger signal size. Subsequently, a smaller series of AE signals indicated that crack propagation occurred intermittently.

The AE signal results show that higher energy is required for the fracture initiation in contrast to crack propagation. The pre-prepared micro-groove was produced with the blunt groove tip. After the first fracture had occurred, a sharp crack tip produced. Greater stress concentration developed at the sharper crack tip in contrast to the blunt groove. Therefore, larger energy was required to increase the local stress at the blunt groove to reach the fracture strength of the material.

3.2.1 Fracture initiation

Fig. 8 shows the influence of laser power on the fracture initiation time. The time taken for fracture initiation to occur has been measured as indicated in Fig. 6(b). It was found that the fracture initiation time decreases with the increase in laser power. For instance, the average fracture initiation times with the laser power of 50 W and 70 W were attained at approximately 0.42 s and 0.27 s, respectively.

The stress force was generated more at higher laser power. Therefore, earlier fracture initiation was achieved with higher laser power.

3.2.2 Intermittent crack propagation

Fig. 9 shows the typical output signals from an AE sensor measured at the middle of the laser path. The result showed that a repetitive AE signal appeared with a starting and stopping phenomena at regular intervals. This occurrence revealed that the crack was extended and frequently relaxed at a perpetual distance. The variation of laser power with the AE signal interval is shown in Fig. 10. The signal intervals were found to be constant and comparable to the laser power. The increase of laser power produced shorter intervals between the crack propagation signals. For instance, the interval of signals found with a laser power of $P=50$ W was about 16.2 ms or 32.4 μm in distance while the signal interval for $P=70$ W was about 10.5 ms or 21 μm in distance. The crack in the material grew with the relaxation of local stress. The crack will develop again when sufficient stress is attained. The stress recovery rate increases with the increase of laser power. Therefore, crack signals appeared rapidly.

3.3 Cleaving surface observation

3.3.1 Cleaving surface at the starting section

Fig. 11 shows the SEM images of the separated surface as observed at the starting area of the silicon wafer.

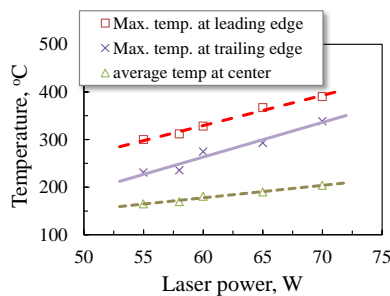


Fig. 7 Influence of laser power on temperature

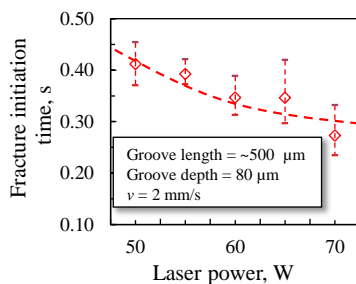


Fig. 8 Fracture initiation time and laser power

A smooth and flat surface was produced with a width of a few micrometres from the wafer's edge followed by a periodic wave marking. This surface was produced due to the initial fracture occurrence at the beginning of the laser irradiation. It was found that the extent of the smooth surface decreased in length with the increase of laser power. The distances of the smooth surfaces were obtained as approximately 420 μm at a laser power of 70 W, in comparison with 295 μm and 185 μm for the laser power of 60 W and 50 W, respectively. The variation of the extent of the smooth surface with the laser power is summarized in Fig. 12.

3.3.2 Cleaving surface at the center section

Fig. 13 shows the SEM images of the cleaving pattern marked on the center section of the cleaving surface. It is shown that constant intervals were developed between the cleaving marks. The distance between the marks decreased with the increase of laser power.

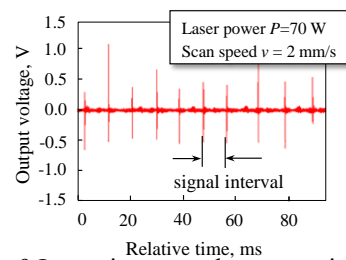


Fig. 9 Intermittent crack propagation signal

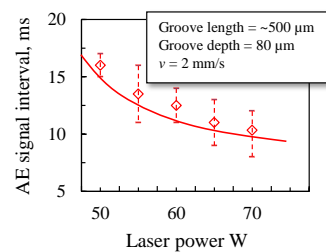


Fig. 10 AE signal interval

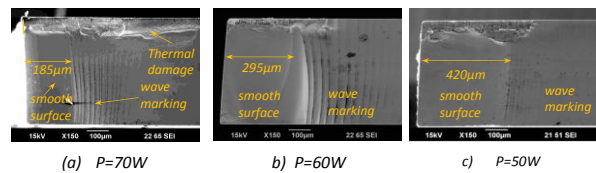


Fig. 11 SEM images at the starting section

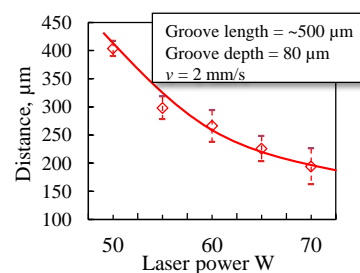


Fig. 12 Smooth surface extent and laser power

The variation of the mark interval and the laser power is given in Fig. 14. The wave marks were developed due to crack advancement occurrences during the intermittent crack propagation phenomena. The interval between the marks was approximately 32 μm with the laser power of 50 W, in comparison with 27 μm and 22 μm for 60 W and 70 W, respectively. The obtained intervals were comparable to the AE signal reported in Fig. 10. The increase of laser power caused higher repetition of the cleaving mark.

3.4 The influences of groove length and depth

The variation of fracture initiation time with groove length and depth are shown in Fig. 15. It was found that the time for fracture initiation was decreased by enlarging the groove length. For instance, the average fracture initiation times obtained with groove lengths of 100 μm and 500 μm are about 450 ms and 270 ms, respectively. Fracture initiation time was also found to be faster for deeper groove depth. The average fracture initiation time with a groove depth of 50 μm was approximately 340 ms compared to 270 ms with a groove depth of 130 μm . It is apparent that the groove has become the point of weakness in the material. Local stress at the groove tip could rise to several times that of the applied stress, and the stress level rose with the increase in groove size.

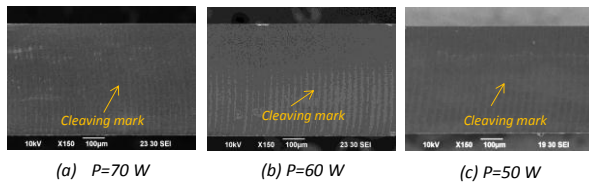


Fig. 13 SEM images at the center section

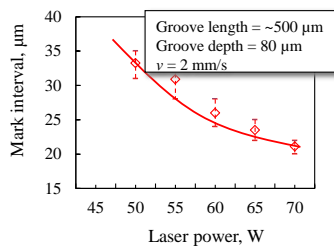


Fig. 14 Cleaving mark's interval and laser power

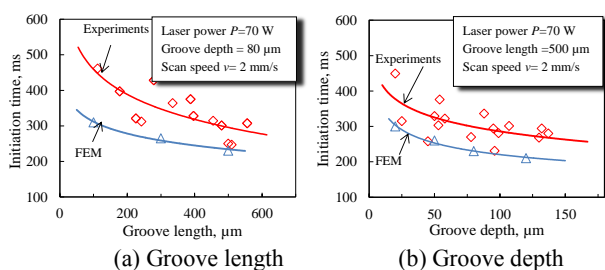


Fig. 15 Comparison of fracture initiation time between experiment and FEM results

4. Finite-element analysis

Finite-element software, ANSYS, was used to analyse the thermal stress during laser irradiation by considering the finite boundary effect. The analysis involved two sequential analyses, namely transient thermal analysis and static structural analysis. Transient thermal analysis was performed by considering the temperature gained from the experimental results.

As the temperature and the thermal stress distribution around the laser spot diverged along the thickness direction of the substrate, the finite-element model was considered as a three-dimensional problem. A silicon wafer specimen with the size of 20 mm x 10 mm x 0.5 mm was used in this study. A micro-groove was modelled at the leading edge of the specimen. The half of the specimen with a coordinate system is illustrated in Fig. 16.

4.1 Analysis conditions

The following basic assumptions for the thermo-mechanical analysis were considered. The material properties such as the heat transfer properties and mechanical properties are assumed to be constant as the temperature range was small. The stress-strain relationship of the Si-wafer is assumed to be perfectly elastic. The surface of x - z plane ($y=0$) is considered to be in adiabatic condition and convection is assumed to exist on all other boundaries. The energy absorption characteristic of the Si-wafer is represented by Beer-Lambert's equation below:

$$\beta = \frac{-\ln T}{x} \quad (1)$$

where T is spectral transmittance ($T=23\%$ as measured experimentally), β is the absorption coefficient and x is the thickness of the wafer. The boundary condition of the structural stress analysis was traction-free on all surfaces, and the x - z surface was set as a fixed plane which has zero displacements in the y -direction. During the laser irradiation, a laser beam was focused on the wafer surface. The laser beam was moving in the x -direction at a constant speed of $v=2$ mm/s. The initial temperature of the Si-wafer substrate and the surrounding temperature were set to 20 $^{\circ}\text{C}$. Table 2 summarizes the analytical condition and properties of the Si-wafer.

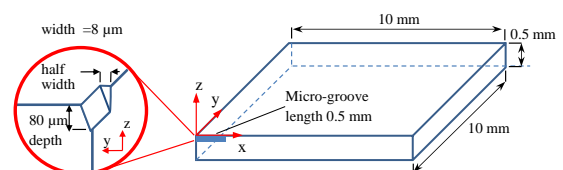


Fig. 16 Half of the specimen and coordinate system

Table 2 Analysis conditions & properties of silicon wafer

Analysis condition		unit
Work piece size	20x10x0.5	[mm]
Laser beam size	0.25 x 0.19	[mm]
Heat transfer coefficient	8	[Wm ⁻² K ⁻¹]
Initial temperature	20	[°C]
Laser beam scan speed	2	[mm/s]
Laser power	70	[W]
Silicon properties		unit
Thermal conductivity	156	[W/m.K]
Specific heat	713	[J/kg.K]
Density	2329	[kg/m ³]
Thermal expansion coef.	2.62 x10 ⁻⁶	[K ⁻¹]
Young modulus	169	[GPa]
Poisson ratio	0.28	

4.1.2 Temperature and thermal stress distribution.

The temperature distributions were calculated at various points in time. Fig. 17 shows the temperature distribution at the times of 0 s, 0.275 s and 0.495 s. The temperature was measured on the surface of the material along the x -axis ($y=0, z=0$). The calculated temperature results were consistent with the temperature from the experimental outcome. Thermal stress σ_{yy} distribution along the x - z plane ($z=-80 \mu\text{m}$) at the time of 0 s, 0.055 s, 0.165 s, 0.275 s, 0.385 s and 0.495 s are shown in Fig. 18.

The stress at the micro-groove tip ($x=0, z=-80 \mu\text{m}$) transformed from a compression to a tensile stress in a short time when the laser beam moved forward in the x -axis direction. This tensile stress σ_{yy} may induce a fracture when the stress intensity factor value reaches the fracture toughness of the material. The fracture is initiated towards the thickness direction (z -axis) and extended through the material.

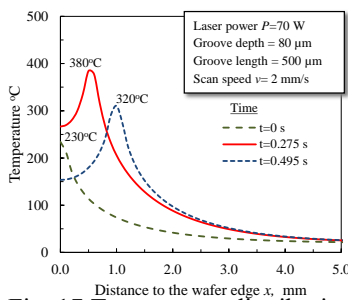


Fig. 17 Temperature distribution

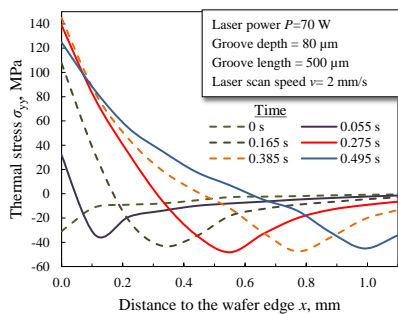


Fig.18 Thermal stress σ_{yy} distribution at various times

4.2 Stress intensity factor

Stress intensity factor, K_I is used to estimate the stress condition in the area of the micro-groove caused by thermal stress induced via laser energy. Irwin found that the stress field $\sigma(r, \theta)$ at the vicinity of a groove tip could be described mathematically as Eq. 2 [9]. In considering that initial fracture occurs according to the crack opening Mode I, K_I can be determined using Eq. 3.

$$\sigma_{yy} = -\frac{K_I}{\sqrt{2\pi r}} \cos \frac{\theta}{2} \left(1 - \sin \frac{\theta}{2} \sin \frac{3\theta}{2} \right) \quad (2)$$

$$K_I = \sigma_{yy} \sqrt{2\pi r} \quad (3)$$

where the σ_{yy} is the magnitude of local stress at distance r from the groove tip, and σ_{yy} is measured at constant $r=20 \mu\text{m}$. During laser irradiation, tensile stress accumulated at the edge of the silicon wafer and concentrated at the position of $x=0, z=-80 \mu\text{m}$. Initial fracture occurs in $-z$ direction due to the existence of the tensile stress gradient. Fig. 19 shows the thermal stress distribution σ_{yy} on x - z plane at the time $t=0.275$ s. The figure on the left displays the σ_{yy} along the $-z$ direction ($x=0$). The variation of thermal stress, σ_{yy} distribution in time, is shown in Fig. 20.

Fig. 21 and Fig. 22 illustrate the relationship between K_I and time for different groove lengths and groove depths. It was found that K_I increases relatively in time until reaching its maximum at approximately $t=0.34$ s.

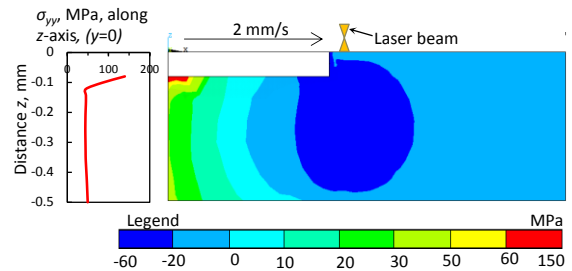


Fig. 19 Thermal stress σ_{yy} distribution on x - z plane at $t=0.275$ s

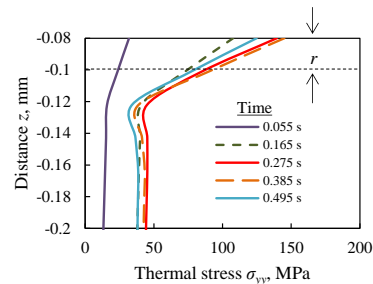


Fig. 20 Variation of thermal stress σ_{yy} in time

When the fracture toughness K_{IC} is achieved, the fracture will be initiated. The result shows that the groove parameters have significant influences on the fracture initiation time. Fracture initiation time is shortened with the increase of groove size. However, the minimum groove size for the achievement of fracture initiation is found to be 100 μm and 20 μm for groove length and depth, respectively.

The variations of fracture initiation time with groove length and depth are shown in Fig. 15(a) and Fig. 15 (b), respectively. It was found that the initiation time decreased with increases in groove length and groove depth. The results were consistent with the experimental results which showed a similar trend between groove size and fracture initiation time. However, fracture initiation was reached faster in the FEM results in contrast to the results of the experiments. This was because during the FEM analyses the ideal conditions were considered, such as ideal boundary conditions, constant material properties and perfect micro-groove model. However, the relationship between fracture initiation and groove parameters was clearly evidenced by experimental and FEM results.

5. Determination of fracture toughness, K_{IC}

The fracture toughness describes the ease with which a fracture or defect is propagated in a material. In this study, fracture toughness K_{IC} of the silicon wafer is estimated using the Vickers indentation technique.

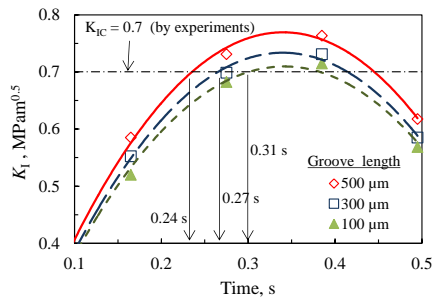


Fig. 21 Stress intensity factor, (K_I) for various groove depths

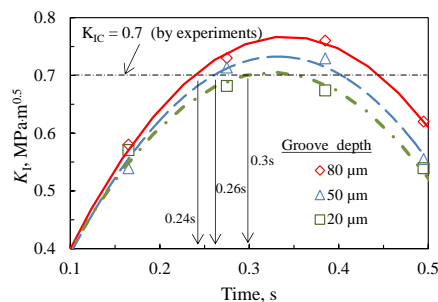


Fig. 22 Stress intensity factor, (K_I) for various groove lengths

The procedure is a simple and cost-effective experiment that relies on the evaluation of the impression left by the indenter on the material. Small surface cracks with controlled size and shape are created by the Vickers indenter. The relation between K_{IC} and the Vickers impression is described as in Eq. 4 [10], where hardness (H_V) is expressed as in Eq. 5.

$$K_{IC} = 0.13 H_V \sqrt{a} \left[\frac{c}{a} \right]^{3/2} \quad (4)$$

$$H_V = 4.5465 \times 10^{-3} \frac{P}{a^2} \quad (5)$$

where K_{IC} is fracture toughness [$\text{MPa}\cdot\text{m}^{0.5}$], H_V is Vickers hardness [GPa], a is the half-diameter of the sample's indentation section [m], c is crack length [m] and P is indentation load [kgf]. The experiment was done according to ASTM C1327-08. Indentation was performed using a micro Vickers hardness testing machine, Akashi HM-101, and the measurement was done using scanning electron microscopy (SEM). Fig. 23 shows an optical micrograph of a 0.3 kgf Vickers indentation in P-type Si-wafer (100) indicating the contact features. Fig. 24 shows the average results of H_V (8.9 GPa) and K_{IC} ($0.7 \text{ MPa}\cdot\text{m}^{0.5}$).

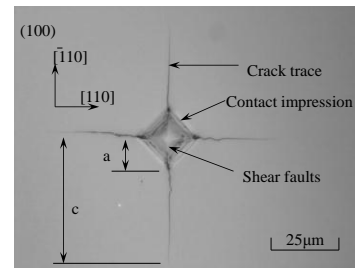


Fig. 23 Optical micrograph of a Vickers indentation

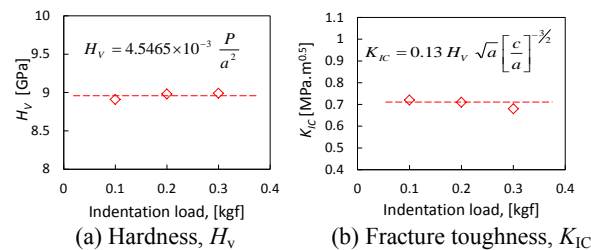


Fig. 24 Hardness, H_V and fracture toughness, K_{IC}

6. Separating mechanism of silicon wafer

Based on the experimental and computational analysis results, the mechanism for separating a silicon wafer by applying a laser beam using the

thermal stress cleaving process can be clearly understood. Fig. 25 illustrates the separating mechanism of the silicon wafer with a pre-prepared micro-groove by utilizing the moving laser beam. The cleaving process can be divided into two stages, namely fracture initiation and intermittent crack propagation.

As shown in Fig. 25(a), when the laser reaches the edge of the wafer, the fracture does not yet occur because the laser beam induces the heat at the laser spot area. Hence, a compressive stress is generated at this point. After the laser beam moves further, the compressive stress transforms into tensile stress. The tensile stress concentrated at the groove tip, and it increases with the rise in temperature at the laser spot and the distance relative to the leading edge of the wafer. When the intense stress at the groove tip reached the material fracture strength, a fracture initiated through the material thickness and extended towards the laser spot in a very short time. As illustrated in Fig. 25(b), the fracture stopped before the laser beam spot and created a new crack tip. Continuous heat supplied by the laser beam caused the tensile stress to increase on the newly created crack tip, and the crack propagated and stopped again before the laser spot. As shown in Fig. 25(c), the cleaving mark was produced as the crack stopped. This process was replicated again and again until the laser beam reached the end of the wafer.

It is demonstrated that fracture initiation and the occurrence of intermittent crack propagation are influenced by the heat supplied from the laser beam during the irradiation process. An increase in laser power improved the fracture initiation time and increased crack propagation recurrence. However, the laser power should be controlled to avoid any thermal damage to the silicon wafer.

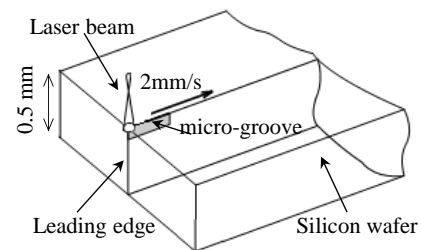
Conclusions

The characteristics of separating a silicon wafer with a moving Nd: YAG laser when using the thermal stress cleaving technique were successfully monitored and analysed by the utilization of a two-color pyrometer and AE sensor. The finite-element (FEM) analysis results explained the stress distribution during laser irradiation. Based on the results gained, the mechanism of the thermal stress cleaving of a silicon wafer with a laser beam was explained.

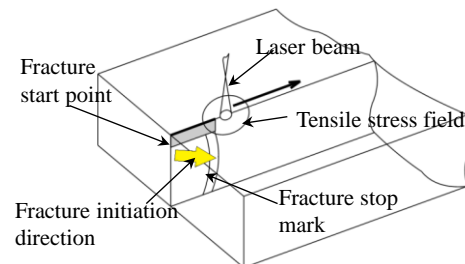
The separating process of the silicon wafer occurred in two stages. The first stage is the fracture initiation, where the fracture occurs due to tensile stress concentrated at the groove tip on the edge of the specimen. The second is intermittent crack propagation, which occurs at constant intervals in time. Fracture initiation and crack

propagation occurrences produced the cleaving mark waves on the separating surface. The cleaving mark wave was consistent with the AE signals.

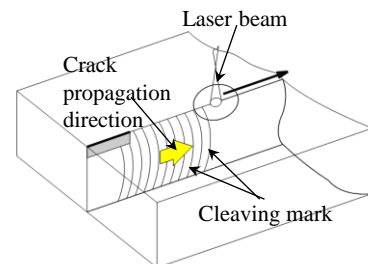
By using FEM, the stress condition has been determined quantitatively by identifying the stress intensity factor K_I . Fracture toughness K_{IC} of the material has been determined experimentally using the Vickers indentation technique. In thermal stress cleaving, a pre-prepared micro-groove is important to control the onset of fracture. The size has significant influence on the fracture initiation time. Therefore, by estimating the stress intensity factor at the groove, the minimum effective dimensions of the micro-groove were suggested.



(a) Laser irradiation start



(b) Fracture initiation



(c) Intermittent crack propagation

Fig. 25 Thermal stress cleaving mechanism of silicon wafer with micro groove

References

- [1] R. M. Lumley. Controlled separation of brittle materials using a laser. *The American Ceramic Society Bulletin*, vol. 48, no. 9, pp. 850-854, 1969.
- [2] E. Lambert, J. L. Lambert, B. D. Longueville. Severing of a glass or vitrocryalline bodies. U. S Patent No. 3935419, 1976.
- [3] C. H. Tsai, C. S. Liou. Fracture mechanism of laser cutting with controlled fracture. *Trans ASME, J. Manuf. Sci. Eng.*, vol. 125, pp. 519–528, 2003.
- [4] T. Ueda, K. Yamada, K. Oiso, A. Hosokawa. Thermal stress cleaving of brittle materials by laser beam. *CIRP Annals - Manufacturing Technology*, 51(1), pp. 149–152, 2002.
- [5] K. Yamada, T. Ueda, A. Hosokawa, Y. Yamane, K. Sekiya. Thermal damage of silicon wafer in thermal cleaving process with pulsed laser and CW laser. In: *Proc. SPIE Laser-based Micro Packaging*, 6107, pp. 61070H–61070H–10, 2006.
- [6] R. Takeda, T. Ueda, T. Furumoto, A. Hosokawa, R. Tanaka. Study on cleaving mechanism of silicon wafer by laser beam irradiation. In: *Proc. Leading Edge Manufacturing in 21st Century (5)*, The Japan Society of Mechanical Engineers, pp. 589-592, 2009.
- [7] T. Ueda, K. Yamada, K. Nakayama. Temperature of work materials irradiated with CO2 laser. *CIRP Ann. - Manuf. Technol.*, vol. 46, no. 1, pp. 117–122, 1997.
- [8] J. Liu, J. Lu, X. Ni, G. Dai, L. Zhang, Y. Chen. Numerical study on thermal stress cutting of silicon wafer using two-point pulsed laser. *Optica Applicata*, 41(1), pp. 247–255, 2011.
- [9] G. R. Irwin. Analysis of stresses and strains near the end of a crack traversing in a plate. *J. Appl. Mech.* 24, pp. 361–364, 1957.
- [10] A. G. Evans, E. A. Charles. Fracture toughness determinations by indentation. *J. American Ceramic Society*, 59: 371–372, 1976.

学位論文審査報告書（甲）

1. 学位論文題目（外国語の場合は和訳を付けること。）

Study on Laser Cleaving Mechanism of Brittle Materials

（レーザによる硬脆材料の割断メカニズムに関する研究）

2. 論文提出者 (1) 所 属 システム創成科学 専攻

(2) 氏 名 Alias bin Mohd Saman

3. 審査結果の要旨（600～650字）

平成26年12月26日に第1回学位論文審査委員会を開催し、提出された学位論文及び関係資料に基づき内容を検討した。さらに、平成27年1月30日に開催した口頭発表会の後、第2回学位論文審査委員会を開催し、協議の結果、以下の通り判定した。

本論文は、硬脆材料表面へのレーザ照射時に生じる熱応力場を利用し、あらかじめ材料表面に導入したき裂を進展させながら分断するレーザ割断について、そのメカニズム解明を目的として理論的かつ実験的にアプローチを行っている。まず、レーザ割断に不可欠な初期溝の導入法として、レーザ照射で生じるアクリル板の熱膨張を利用したマイクロレンズ製作手法を提案し、同マイクロレンズを用いた加工により、硬脆材料表面に熱影響層が殆ど無い良好な深溝形状を創製する技術を確認した。次に、得られた深溝を初期き裂として用いた割断について、レーザ照射時の試料表面温度やAE波を測定し、有限要素解析による材料内部の温度および応力分布も併せ、材料のき裂進展性を詳細に検討した。そして、き裂進展がレーザ出力や初期溝形状に大きく依存すること、また、レーザ照射にともなって材料表面が破壊じん性値を超える温度に達するとき裂が進展することを理論的かつ実験的に示した。加えて、特性の異なる複数の材料との比較から、材料に対するレーザの吸収特性によってき裂進展形態が異なる事も明らかとした。

以上のように、本論文はレーザによる硬脆材料の割断メカニズム解明に関して有用なデータを示し、工学的な寄与も大きく、博士(工学)の学位に値すると判定した。

4. 審査結果 (1) 判定 (いずれかに○印) 合格・不合格

(2) 授与学位 博士(工学)